UC Davis

UC Davis Electronic Theses and Dissertations

Title

D-band Wideband Planar Antenna Design

Permalink

https://escholarship.org/uc/item/6g83t831

Author

Han, Peixin

Publication Date

2024

Peer reviewed|Thesis/dissertation

eScholarship.org Powered by the California Digital Library
University of California

D-band Wideband Planar Antenna Design

By

PEIXIN HAN
THESIS

Submitted in partial satisfaction of the requirements for the degree of

MASTER OF SCIENCE

in

Electrical and Computer Engineering

in the

OFFICE OF GRADUATE STUDIES

of the

UNIVERSITY OF CALIFORNIA

DAVIS

Approved:

_____

Qun Jane Gu, Chair

_____

Omeed Momeni

_____

Juan Sebastian Gomez-Diaz

Committee in Charge

2024

List of Abbreviation

PMMW – Passive Millimeter Wave

CPW – Coplanar Waveguide

GCPW – Grounded Coplanar Waveguide

HFSS - High Frequency Structural Simulation

SIW – Substrate Integrated Waveguide

List of Figures

CONTENTS

Abstract

Passive millimeter wave (PMMW) is becoming increasingly popular for signal detection. However, it suffers from the attenuation during the propagation. Among all frequency windows, D-band PMMW has lowest attenuation in propagation within oxygen, water, fog and drizzle. The purpose of this research is to design wideband antennas for D-band passive millimeter wave imaging system with good gain performance and wide impedance bandwidth.

The thesis presents two planar antennas for passive imaging systems. Both antennas are designed in D-band (140GHz) and are excited by *Coplanar Waveguide* (CPW). Both antennas are constructed using a low permittivity material, quartz (ϵ_r = 3.78). The first design is a planar monopole antenna, which can provide large impedance bandwidth (97-226GHz) due to characteristics of the planar monopole antenna. However, the leakage of back radiation decreases the gain of planar monopole antenna. The second antenna, coplanar patch antenna, is introduced to increase the gain within desired frequency range. By incorporating a back ground plane, the proposed coplanar patch antenna achieves 49.15 GHz -10dB impedance bandwidth (115.56 to 164.71 GHz) with a minimum gain larger than 4.8 dBi. Parametric sweepings are done to optimize the antenna performance, and corresponding discussions about the influences by those parameters are included. Both antennas can cover the desired frequency window with good gain performance, making them suitable for PMMW imaging system.

Acknowledgements

First and foremost, I would like to express my deepest gratitude to Professor Qun Jane Gu for her invaluable guidance, unwavering support, and assistance throughout my master's program. Her insights and research methodologies have profoundly shaped my academic journey. I am sincerely appreciative of the opportunity she provided me to join HSICS lab and participate in this project. Without her mentorship, this thesis would not have been possible.

I am also grateful to the PhD students in our HSICS lab at the University of California, Davis—Hai Yu, Sajjad Sabbaghi Saber, Zahra Mohseni, and Mohammad Bagher Ghiasi—for their guidance and support in resolving various technical challenges.

I wish to extend my sincere appreciation to Dr. Omeed Momeni and Dr. Gomez Diaz Juan for serving as members of my thesis committee.

I am deeply thankful to Dr. Anh-Vu Pham and his PhD student, Kajol Chandra Paul, for their overwhelming assistance in this research on antenna design. I would also like to express my gratitude to Dr. Xun Gong from the University of Central Florida and his PhD student Zahid Hasan for their valuable technical support for this thesis.

A special thanks to UC Davis for providing a remarkable environment to work and study alongside such experienced faculty, staff, and engineers.

Finally, I want to express my love and gratitude to my parents for their unwavering support in helping me reach this milestone.

Chapter 1 Introduction

1.1 PMMW Imaging System

Passive imaging is widely used in industry, especially for detection, since it can receive signals without transmitter. *Passive millimeter-wave* (PMMW) imaging is a highly promising candidate for passive detection due to its ability to penetrate various low-visibility objectives.

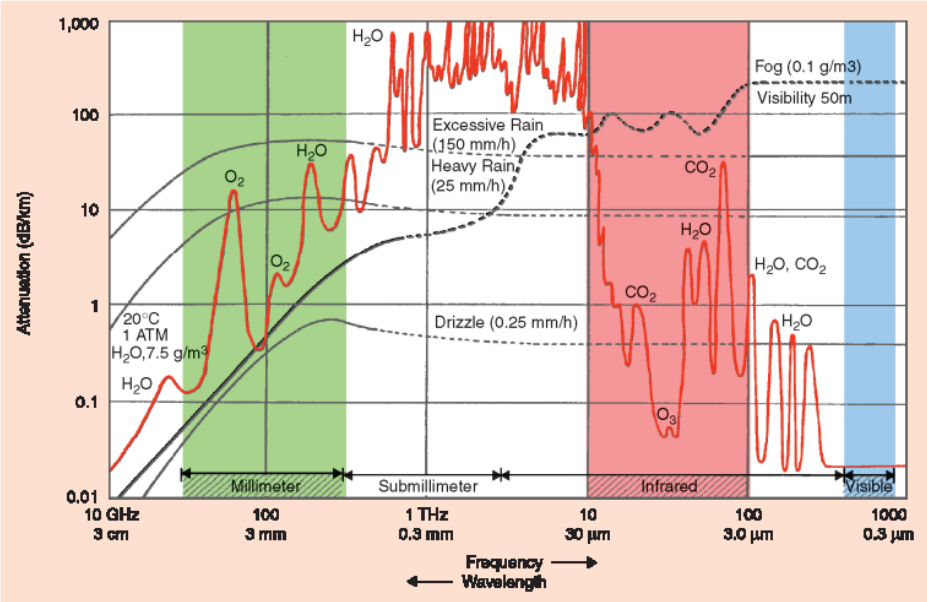

Figure 1.1 The attenuation of millimeter waves by atmospheric gases, rain, and fog

1.2 D-band PMMW Imaging

Figure 1.1 from shows the attenuation for electromagnetic wave within different frequency windows [1]. Compared to submillimeter waves, infrared waves and visible waves, millimeter waves experience lower loss during propagation. Among available

frequency windows, D-band (140 GHz) millimeter exhibits relatively small attenuation when propagating through oxygen, water, fog and drizzle, which makes it particularly advantageous. A passive imaging system with D-band PMMW detection can be promising in future applications. This thesis will mainly focus on the design for D-band PMMW antennas. Compared to low frequency antennas, the design of D-band antennas is more challenging due to multiple factors, such as gain and bandwidth, which will be introduced in Section 1.3.

1.3 Challenges in D-band Antenna Design

Some requirements make the design of D-band antenna design challenging:

1. *Antenna Performance:* The low level of blackbody radiation for detection requires the receiving antenna with high-gain and excellent impedance matching within the proposed frequency range, posing a significant challenge for D-band antenna design.
2. *Fabrication Complexity***:** The design procedure must consider the fabrication complexity aspects. Some structures, such as dipole antenna, is hard to fabricate for millimeter wave application. However, planar structure takes advantage of its ease of fabrication and integration. Planar structure, such as microstrip patch antenna (MPA) and slot antenna, can be easily fabricated trough etching. The design procedure should also consider the yield of manufacturing. During the design, the limitation of equipment should be seriously considered. For example, in author's case, gaps or slots

lower than 15 μm will be challenging for etching on the proposed substrate material, quartz.

3. **Integration Concern.** D-band antennas are usually considered to connected with chip even integrated to the chip in some cases, which requires the antenna to be readily connectable to the front-end circuits and measurement equipment. Considering the simplicity of fabrication and connection, 50Ω coplanar waveguide (CPW) feedline is used as the transmission line between the antenna and the measurement equipment.

1.4 Thesis Layout

In this thesis, two types of planar antennas for D-band PMMW imaging applications are designed and simulated by using High Frequency Structural Simulation (HFSS). This thesis is organized as follows. In Chapter 2, basic terminologies and some classical antennas are introduced. Chapter 3 gives a brief literature review of D-band antennas. The design procedure and simulation results of the planar monopole antenna are described in Chapter 4. However, the gain of this antenna is reduced because of the back radiation. To increase the gain, a back ground plane is placed behind the substrate to reduce the back radiation. This antenna is known as coplanar patch antenna and its design procedure and simulation results are introduced in Chapter 5. Finally, the thesis ends with Chapter 6 about a brief conclusion and the avenues for future work exploration.

1.5 Conclusion

This chapter first introduced the desirable future of PMMW. Among all millimeter wave frequency windows, D-band is the most suitable window due to its low attenuation during the propagation in common environment. However, there are only a few suitable wideband D-band antennas. The consideration of antenna performance, commercialization and ease of connection, antenna design for D-band is challenging. Next chapter gives a brief introduction of basic terminologies and some classical antenna which motivates our proposed antenna design.

Chapter 2 Antenna Theory, Impedance Matching, CPW, Software Introduction

2.1 Antenna Theory

Antennas play important roles in wireless applications, serving as the key elements to receive electromagnetic waves from air or other medium and transmit signals into those environments. The performance of the antenna can be assessed by several parameters, such as radiation pattern, gain, directivity and impedance bandwidth.

2.1.1 Radiation Pattern

The radiation pattern of antenna represents spatial distribution of radiated energy, which illustrates how an antenna radiates energy into surrounding environment. It is usually normalized and plotted as polar or Cartesian coordinates in decibel (dB).

2.1.2 Gain and directivity

The gain of the antenna is defined as the ratio of the radiated power in a specific direction to the power that will be radiated if the received power is isotopic. Directivity is closely related to antenna gain and it is defined as the ratio of radiated power in a certain direction over the radiated power if the transmitted power is isotropic. The primary distinction between gain and directivity is, gain accounts for the total power consumption of the antenna, while for directivity it considers the total transmitted power. Both

parameters provide insights to the radiation distribution, but unlike the directivity, gain is also influenced by antenna efficiency.

2.1.3 Bandwidth, Impedance Matching

Bandwidth refers to the frequency range over which the antenna satisfies specific performance criteria. One of the most widely adopted criteria to define the bandwidth is impedance bandwidth. In this thesis, -10dB impedance bandwidth is utilized to assess the antenna performance. Millimeter wave measurement usually use port with $50\ \Omega$ impedance to balance minimal power loss with optimal power transfer. To achieve efficient power transfer, it is essential to ensure impedance matching between the port and the antenna.

2.2 Classical Antennas

2.2.1 Dipole Antenna: Wire Dipole and Planar Dipole

The dipole antenna is one of the simplest and most widely used antenna types. It consists of two radiating conductors connected by an excitation source. Figure 2.1 illustrates a traditional wire dipole antenna with resonant frequency of 140GHz. In this configuration, two cylindroid conductors are connected by a lumped port represented by a purple square. The resonant frequency of the dipole antenna is primarily determined by the length of the cylindroid conductors. A commonly used type of dipole antenna is half-wavelength dipole antenna, where the total electrical length of two conductor is equal to half of the wavelength. Here λ_0 is the free-space wavelength for wire dipole antenna as shown in Equation (2.1). The electric field and magnetic field distribution is illustrated as

Figure 2.2. The maximum electric field happens at two ends of the dipole while the maximum magnetic field happens at the center of the dipole antenna.

$$L = \frac{\lambda_0}{2} \tag{2.1}$$

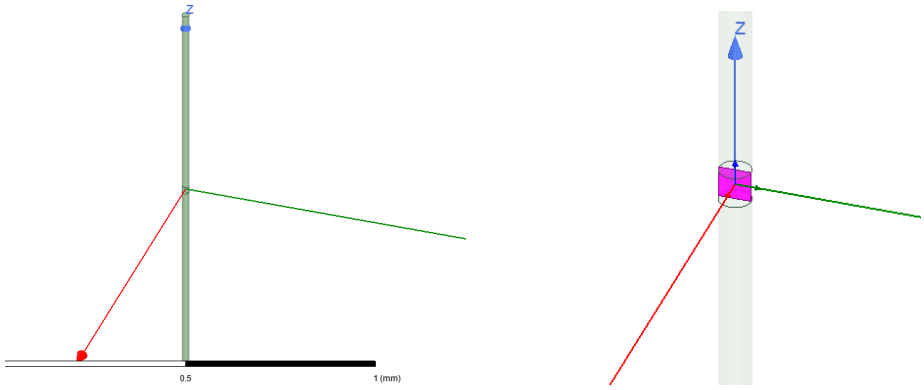

Figure 2.1 140 GHz wire dipole antenna. The left one is the overview of the whole antenna. The right one shows the lumped port excitation.

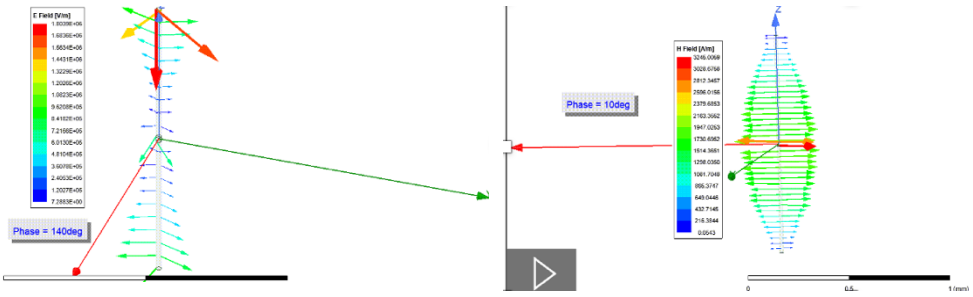

(a) E field (b) H field

Figure 2.2 140 GHz wire dipole antenna field distribution. (a) illustrated the Electric field distribution and (b) shows the magnetic field distribution.

Planar dipole antenna is revolved from wire dipole antenna due to the advantages of planar structures indicated in Chpater1. The planar dipole antennas are always placed on the top of the substrates, which can increase the firmness of the antenna. Figure 2.3 is a simple planar dipole antenna excited by a lumped port. The wavelength is varied due to the exisitance of the substrate. Different from the half free-space wavelength calculation shown in Equation (2.1), planar radiating conductor's length is determined as Equation (2.2-a) and (2.2-b). Here λ_p is the effective wavelength considering the substrate, ϵ_r is the permittivity of the substrate, L_p is the effective electrical length. The length of the planar dipole antenna in Figure 2.3 equals to $613\mu m$.

$$\lambda_p = \lambda_0 \sqrt{\frac{2}{\epsilon_r + 1}} \qquad (2.2-a)$$

$$L_p = \frac{\lambda_p}{2} \qquad (2.2-b)$$

Figure 2.4 inllustrates the Electric and magenetci field distribution of the planar dipole antenna at 140 GHz for quartz substrate ($\epsilon_r = 3.78$). The field distribution of the planar dipole antenna is similar to that of the wire dipole antenna.

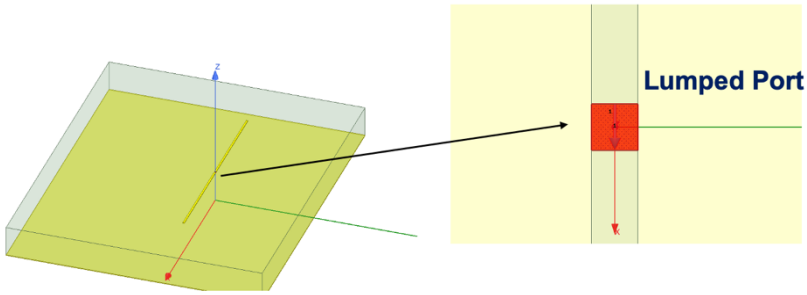

Figure 2.3 140 GHz planar dipole antenna. The left one is the overview of the whole antenna. The right one shows the lumped port excitation

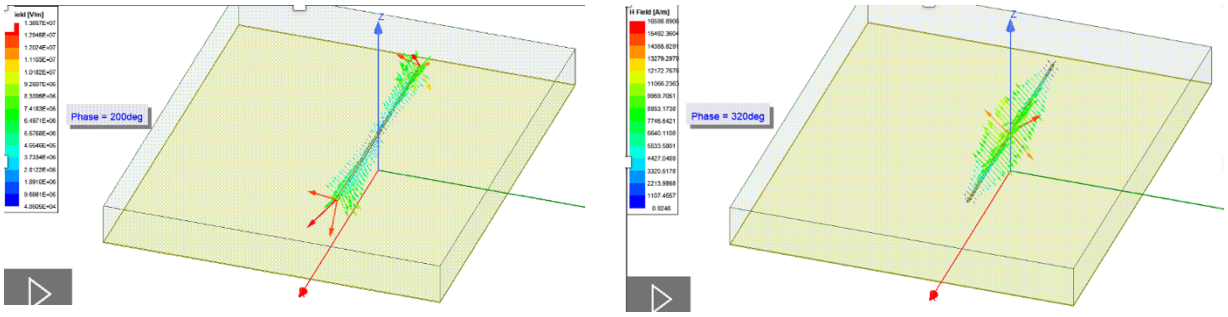

(a) E field (b) H field

Figure 2.4 140 GHz planar dipole antenna field distribution. (a) illustrated the Electric field distribution and (b) shows the magnetic field distribution.

2.2.2 Microstrip Patch Antenna

Microstrip patch antennas are widely used in commercial applications due to their ease of fabrication and integration. A microstrip patch antenna typically consists of a radiating patch, a substrate and ground plate on the other side. The patch can be fed by

various methods, including microstrip feedline and coaxial feedline. The shape of the patch can be various, such as rectangle, circle. Figure 2.2 shows a 2.4GHz microstrip rectangular patch antenna with microstrip feedline. The performance of the microstrip patch antenna is primarily determined by several parameters, such as the size of the patch and the thickness of the substrates. Among all these parameters, the length of the radiating patch is the main factor that determines the antenna's resonant frequency.

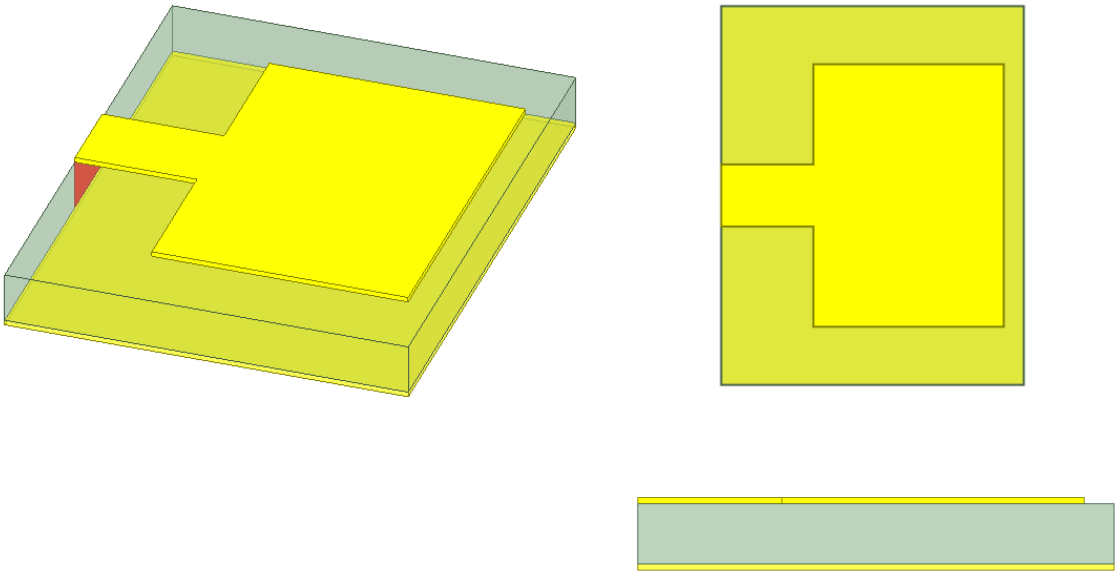

Figure 2.5 2.4 GHz microstrip patch antenna

The electromagnetic wave propagates in the metal patch primarily in the TM_{010} mode as illustrated in Figure 2.6, which necessitates the length of the patch to be approximately half the wavelength. However, the fringing effect at the edge of the patch

increases the effective length, consequently influencing the resonant frequency. The relationship between the patch length and the frequency is described by Equation (2.1) - (2.4), where ϵ_r is the permittivity of the substrate and ϵ_{reff} is effective permittivity. As frequency increases, ϵ_{reff} approaches to ϵ_r, since more electric field lines concentrate within the substrate. The theoretical value of the patch length can be considered as the summation of half the wavelength, L, and the extended length due to the fringing effect ΔL, as expressed in equation (2.4).

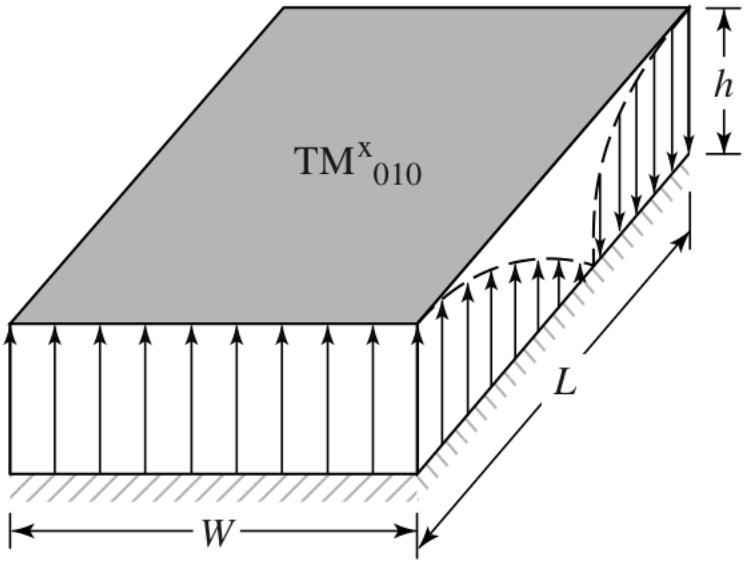

Figure 2.6 TM_{010} for microstrip patch antenna [2]

$$\epsilon_{reff} = \frac{\epsilon_r + 1}{2} + \frac{\epsilon_r - 1}{2}\left(1 + 12\frac{h}{W}\right)^{-\frac{1}{2}} \tag{2.1}$$

$$\Delta L = 0.412h\frac{\left(\epsilon_{reff} + 0.3\right)\left(\frac{W}{h} + 0.264\right)}{(\epsilon_{reff} - 0.258)(\frac{W}{h} + 0.8)} \tag{2.2}$$

$$L = \frac{\lambda}{2} \tag{2.3}$$

$$L_{eff} = L + 2\Delta L \tag{2.4}$$

Although the microstrip patch antenna takes advantage of the ease of fabrication and connection, the bandwidth is typically limited.

2.3 Software Issues

2.3.1 Software Introduction

High Frequency Structural Simulation (HFSS) - HFSS is a high frequency simulation tool for electronic components. In this thesis, HFSS is used to simulate the electromagnetic properties of our proposed antenna.

2.3.2 Port Selection

In HFSS simulation, the antenna is activated by a specific source, which is known as “port”. Various types of commonly used ports are provided in HFSS simulation, including lumped port and wave port. The wave port requires port size to be large enough to cover the whole measuring surface, making it less suitable for planar antenna simulations in this thesis. However, wave ports are more widely utilized in waveguide simulations. In this thesis, lumped ports are employed to excite the antennas with the impedance set to 50 Ω to simulate the measurement equipment port. In this thesis, all the lumped ports are configured as rectangles with red or purple colors, such as the purple rectangle in Figure 2.1.

2.3.3 Adaptive meshing

For HFSS simulation, the initial step for computation is separating the complex structure into smaller analyzable elements, which is known as meshing. The accuracy of the simulation increases with an increased number of mesh elements. However, this also leads to greater model complexity and longer simulation times. To optimize the performance, the adaptive meshing is employed in HFSS simulation, which can accelerate the simulation process. HFSS incrementally increases the number of meshes and calculates the change in the S-parameter (δ) at the frequency where adaptive meshing is applied during each iteration. If the S parameter fails to converge, the meshing number continues to increase. This technique allows the software to enhance the mesh density more efficiently. It is important to note that adaptive meshing settings must be handled with care. Some deceptive cases might happen if the settings are incorrect. For example, the adaptive meshing might stop prematurely since δ is smaller than the threshold value, even though the S parameter is not truly convergent. In such cases, correspondingly increasing the minimum number of passes can compel the adaptive meshing to continue for additional iterations, ensuring more accurate results.

2.4 Conclusion

Some basic terminologies about antenna are introduced in this chapter. Some fundamental antenna performance evaluation parameters are first introduced. Parameters like radiation pattern, gain and directivity are used to evaluate the radiation performance,

while parameters such as impedance bandwidth evaluate the antenna transmission efficiency. Dipole antenna and microstrip patch antenna are two classical antennas. To simulate those antennas, HFSS is used in this thesis, while some settings of HFSS are worth discussing. Port selection is important and lumped ports are used in this thesis. Adaptive meshing is applied in HFSS simulation to accelerate the simulation times, which needs carefully setting to guarantee the accuracy of the results. The next chapter will discuss about transmission lines that connected the ports and the antennas.

Chapter 3 Transmission Line

As discussed in Chapter 1, the planar structures are more preferred in D-band antenna design due to its ease of integration and fabrication. Microstrip lines and Coplanar Waveguides (CPW) are two commonly used planar feeding structures in antenna design. A crucial aspect of the antenna design process is ensuring the characteristic impedance of the feedline is properly optimized. The input impedance of the antenna should be tuned to 50 Ω to maximize transmission efficiency and minimize loss. By matching the characteristic impedance of the transmission line and the antenna's input impedance to 50 Ω, the entire antenna system achieves optimal impedance matching. In this chapter, two classical transmission line structures are introduced, along with some determinant equations necessary for characteristic impedance calculation.

3.1 Microstrip Transmission Line

Microstrip line consists of a signal trace, a substrate and a ground plane. The cross-section configuration of the microstrip is shown in Figure 3.1. The electromagnetic wave travels in the microstrip line in the quasi-TEM mode. The characteristic impedance can be determined by following equations [3]:

$$\epsilon_e = \frac{\epsilon_r + 1}{2} + \frac{\epsilon_r - 1}{2} \frac{1}{\sqrt{1 + \frac{12d}{W}}}. \tag{3.1}$$

$$Z_0 = \begin{cases} \frac{60}{\sqrt{\epsilon_e}} \ln\left(\frac{8d}{W} + \frac{W}{4d}\right) & \text{for} W/d \leq 1 \\ \frac{120\pi}{\sqrt{\epsilon_e}\left[\frac{W}{d} + 1.393 + 0.667 \ln\left(\frac{W}{d} + 1.444\right)\right]} & \text{for} W/d \geq 1. \end{cases} \quad (3.2)$$

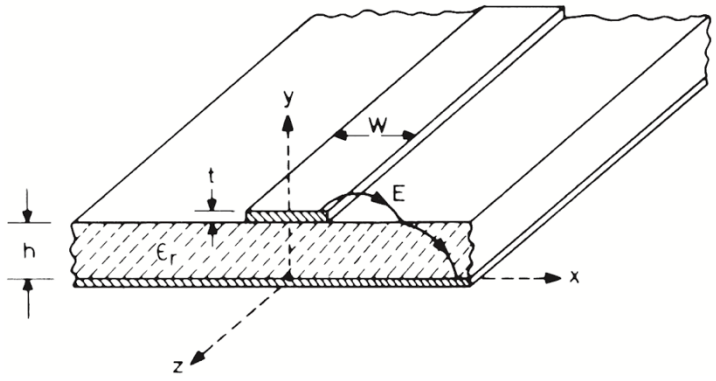

Figure 3.1 Microstrip line[4]

3.2 Coplanar Waveguide (CPW)

The coplanar waveguide (CPW) is a preferred transmission line for planar antenna design due to its advantageous structure. Unlike the microstrip line, which uses a single signal trace on the substrate's surface, CPW features two ground planes flanking the signal trace. The structure of the CPW line is shown in Figure 3.2. Compared to the microstrip line, CPW offers better connectivity since it places both signal trace and the ground plane on the same surface, making it easy to integrate with the MMIC circuits [5]. In this thesis, CPW is employed as the feedline to excite the antenna.

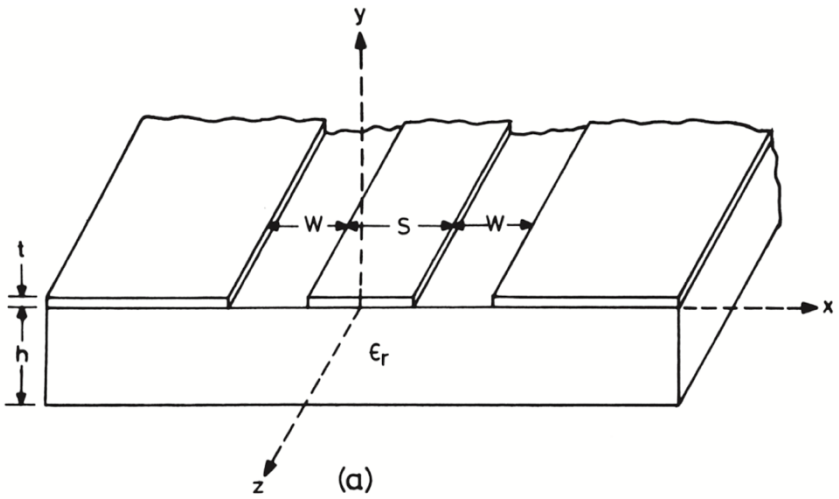

Figure 3.2 Cross view of CPW[4]

Similar to the microstrip line, the characteristic impedance of CPW can be adjusted by changing material of the substrate (change ϵ_r). In wideband antenna design, the substrate material is mainly determined by the requirement of the bandwidth performance. The characteristic impedance of CPW, as expressed in the Equation (3.3) is primarily determined by both permittivity of the substrate (ϵ_r) and the physical dimension of the gap and the trace width. As the ϵ_r is determined, the characteristic impedance of CPW can be adjusted by varying the factor k_1, which is the ratio of the signal trace width (S) to the distance between two ground planes ($S + 2W$) [4]:

$$Z_0 = \frac{30\pi}{\sqrt{\varepsilon_{\mathrm{re}}}} \frac{K'(k_1)}{K(k_1)} \tag{3.3}$$

$$\frac{K(k)}{K'(k)} = \frac{\pi}{\ell n\left[\frac{2\left(1+\sqrt{k'}\right)}{1-\sqrt{k'}}\right]} \quad \text{for} 0 \le k \le 0.707$$
$$\frac{K(k)}{K'(k)} = \frac{1}{\pi}\ell n\left[\frac{2\left(1+\sqrt{k}\right)}{1-\sqrt{k}}\right] \text{for } 0.707 \le k \le 1 \qquad (3.4)$$
$$k' = \sqrt{1-k^2}$$

$$k_1 = \frac{S}{S+2W}$$

Frequency sweeping is applied to the CPW structure to evaluate its performance. In Although equation (3.4) indicates the characteristic impedance is independent of the frequency, higher order modes might affect the performance of the CPW feedline within high frequency range. To assess whether the characteristic impedance of the CPW feedline varies across D-band frequency range, the configuration shown in Figure (3.3) is simulated in HFSS. In the setup, the CPW feedline is connected to two lumped ports.

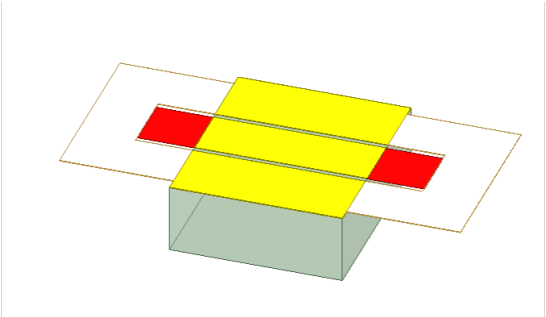

Figure 3.3 CPW structure

The simulation results are exported to Candence for further analysis. Two 50 Ω ports are connected to a NPORT element, with the S-parameters imported. By constructing the

circuit depicted in Figure 3.4, the impedance measurement values can be extracted and the characteristic impedance can be calculated by using Equation (3.5).

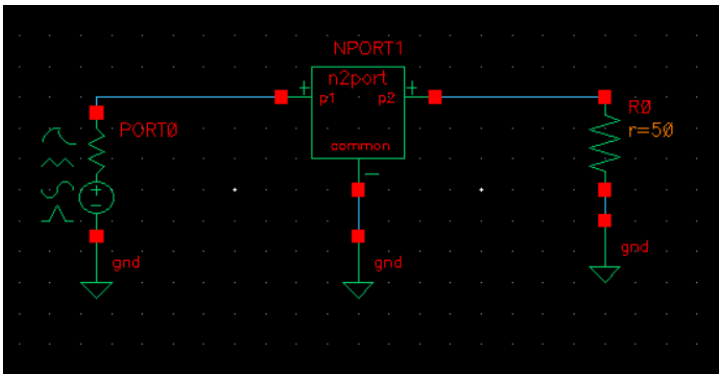

Figure 3.4 CPW impedance measurement circuit in Cadence

$$Z_{in} = Z_o \left[\frac{Z_L + jZ_o \tan(\beta l)}{Z_o + jZ_L \tan(\beta l)} \right] \tag{3.5}$$

The figure of characteristic impedance with frequency sweeping is illustrated as Figure 3.5 which is generated by MATLAB. This figure shows that the characteristic impedance of the CPW feedline remains stable around 50 Ω, demonstrating its suitability for D-band antenna design.

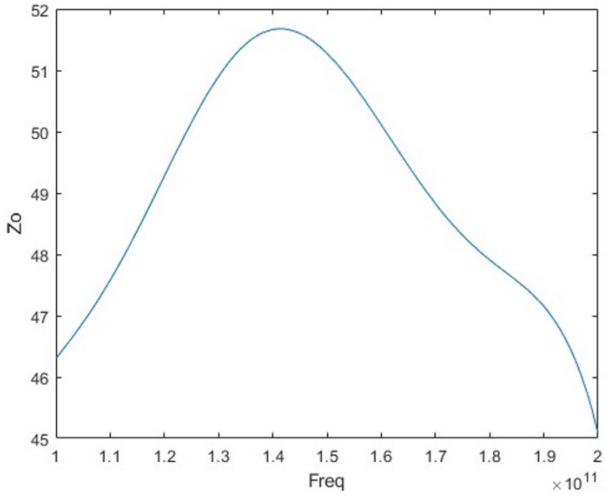

Figure 3.5 Characteristic impedance with frequency sweeping

In Chapter 5 and 6, both proposed antenna structures use CPW-fed configuration. However, the coplanar patch antenna introduced in Chapter 6 differs from the CPW shown in Figure 3.1. The CPW used in coplanar patch antenna has a ground plane at the bottom, which is known as *grounded coplanar waveguide* (GCPW). This difference affects the characteristic impedance calculation. In this thesis, parametric sweeping is employed to accurately determine the parameters for achieving 50 Ω GCPW feedline.

3.3 Conclusion

Transmission line is a crucial part of planar antenna design. In this chapter, two fundamental transmission line structures, the microstrip line and CPW, are introduced. A simulation about verification of the 50 Ωcharacteristic impedance for CPW is performed

by using HFSS, Cadence and MATLAB. The next chapter provides a review about related antenna.

Chapter 4 Antenna Review Survey

This chapter reviews the current state-of-art in D-band antenna design. According to [6], current D-band antenna structures can be categorized based on the fabrication and packaging technique: on-chip antennas, on-chip antennas with modifications, antenna-in-package, low temperature co-fired ceramics, metallic antennas, PCB-antennas, 3-D printed antennas and other antennas. For this thesis, the proposed antennas fall under the category of PCB antennas. Compared with the categories, PCB antennas have relatively low fabrication cost. Although 3-D printed antennas provide advantages such as short fabrication time and low fabrication costs, they are not considered in this thesis due to limitations in available fabrication equipment. Other D-band antenna categories, such as on-chip antennas, have more complex structures and high fabrication cost and time, making PCB-antennas the more suitable option for this thesis.

In addition to fabrication and packaging methods, D-band antennas can also be classified based on their structural configurations. Various related planar designs have been reported. For instance, Ma introduces a D-band antenna design with substrate integrated waveguide (SIW) feedline, discussing both horn and patch antenna structures [7]. The SIW uses two rows of via holes along the signal trace for guidance. Although both antennas are powered by SIW feedline, the planar patch antenna emerges as a more desirable candidate compared to the horn antenna. This SIW-fed patch antenna provides wide -10 dB impedance bandwidth (129.5 GHz to 156.5 GHz) and impressive peak gain (15.4 dBi at 140 GHz). Another notable design is a Y-shaped open-ended microstrip

antenna introduced in [8] which is fed by the coplanar waveguide and consists of two narrow open-ended microstrip antennas, achieving 13.6 dBi gain with 20 GHz bandwidth. Furthermore, in [9], a waveguide-to-coplanar waveguide transition with D-band wideband patch antenna is introduced. This article demonstrates a novel structure of coplanar patch antenna with a U-slot at the center of the patch. This antenna achieves 50.5 GHz impedance bandwidth and 7.4 dBi peak gain at 140GHz. This structure inspires the improvements of microstrip patch antenna introduced in Chapter 6. However, the detailed design procedure is not fully demonstrated in that article and only the peak gain is illustrated. The design procedure is challenging and warrants discussing, which will be discussed in Chapter 6 of this thesis. Also, the minimum gain within that frequency range is not listed, which makes this antenna questionable for wideband applications. For wideband antenna design, it is crucial that the gain remains consistent across the operating frequency range, making the minimum gain within that range an important consideration.

Some antennas operating in several GHz frequency ranges also serve as valuable references for D-band antenna design. A multiband antenna with excellent radiation characteristics and large impedance bandwidth is demonstrated in [10]. Designed for WLAN/WiMAX communication, this CPW-fed planar monopole antenna features a ring slot at the center of the planar monopole patch. This antenna design achieves a low bandwidth from 2.34 to 2.42 GHz centered at 2.38 GHz and an upper bandwidth from 3.16 to 6.57 GHz with two resonant frequencies of 3.5 and 5.38 GHz, which covers the

WLAN/WiMAX communication frequency range. Although the operating frequency of this antenna differs from that used in PMMW imaging, the innovative design of this planar monopole antenna has inspired the development of our D-band planar monopole antenna. The wideband characteristics of this CPW-fed planar monopole antenna make it a strong candidate for adaptation to D-band antenna design, as discussed in Chapter 5.

Chapter 5 Planar Monopole Antenna

5.1 Motivation

As discussed in Chapter 2, dipole antenna is widely utilized in industry because of its simplicity of fabrication. Monopole antenna, derived from dipole antenna, replaces half of the radiating conductor with ground plane. By imaging theory introduced in [2], quarter-wavelength monopole antenna can be derived from half-wavelength dipole by regarding the ground plane as a "mirror". The relation between resonant frequency and the patch width L_p is illustrated as Equation (5.1).

$$L_p = \frac{c}{4\, f_r \sqrt{\frac{\epsilon_r + 1}{2}}} \tag{5.1}$$

Planar monopole antenna inherits relatively high impedance bandwidth characteristic of dipole antenna. In [11], the planar monopole antenna with rectangular shape patch can achieve 75% impedance bandwidth in S-band, which is inspiring for wideband application. Compared to traditional wire conductor as the radiating component, planar patch can provide a more compact and integrated solution when it is used as the radiating component in monopole antenna design.

In [10], a CPW-fed planar monopole antenna with a circular slot etched is introduced for WLAN/WiMAX. This antenna has two frequency band for WLAN/WiMAX. The first resonant frequency at 2.45 GHz is generated by the circular slot etched on the radiating patch, while the second frequency band starting from 3.27 to

6.59 GHz is achieved by the planar monopole antenna itself. The second frequency band is noteworthy as it demonstrates the inherent characteristic of planar monopole antenna, including wide bandwidth and acceptable gain for wireless communication, which is particularly inspiring for D-band antenna design.

5.2 Material Selection

In D-band antenna design, the selection of the material of the substrate is crucial, as it directly affects the impedance bandwidth. A review by Gupta highlights that the bandwidth of the microstrip patch antenna is influenced by the permittivity of the substrate, its lower permittivity contributing to increased bandwidth [12]. Both antennas in this thesis are designed with quartz, which characterized by its low permittivity ($\epsilon_r = 3.78$) and low loss (loss tangent = 0.0002). All the metallic components, including the signal trace, ground plane and the patch, are designed with gold. This material combination is also employed in the coplanar patch antenna design, which will be introduced in Chapter 6.

5.3 Design and Analysis

The whole planar monopole antenna composes of a planar monopole and a 50 Ω CPW feedline. The structure of coplanar patch antenna is shown in Figure 5.1. The red square with length S is the lumped port used to excite the whole antenna optimized parameter values are listed as Table 5.1.

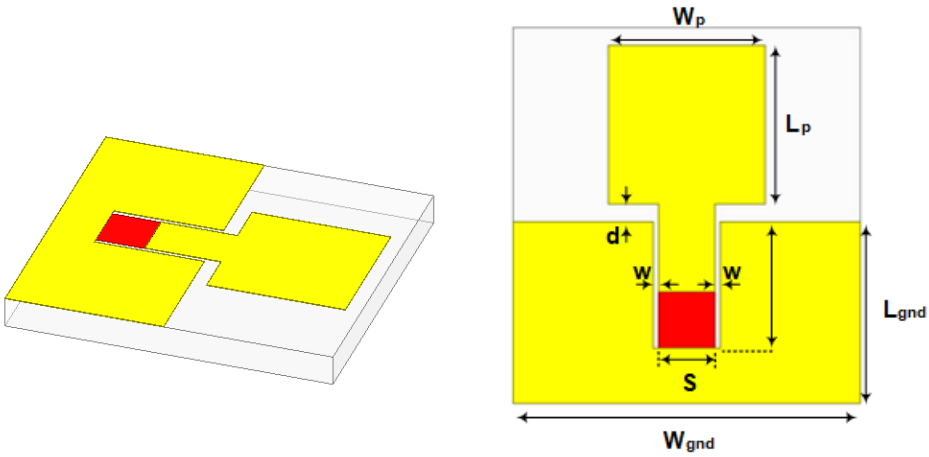

Figure 5.1 Planar monopole antenna structure

Parameter	Value (μm)	Parameter	Value (μm)
W_p	446.2	L_p	455
W_{gnd}	990	L_{gnd}	495
w	15	s	160
d	50	/	/

Table 5.1 Parameters for planar monopole antenna

The simulation results are shown as Figure 5.2, 5.3. This antenna provides wide impedance bandwidth (97-226GHz) but exhibits a relatively low gain (2.2 dBi). The -

10dB bandwidth is sufficiently broad to cover the PMMW frequency window (120 GHz to 160 GHz). However, the maximum gain is limited due to the leakage of the back radiation. To mitigate this leakage, a ground plane can be added to the back of the substrate, transforming the design into a CPW-fed microstrip patch antenna. The microstrip patch antenna has consistently been limited by its low bandwidth, necessitating the introduction of our second proposed antenna, the coplanar patch antenna, to enhance bandwidth performance, which will be discussed in Chapter 6.

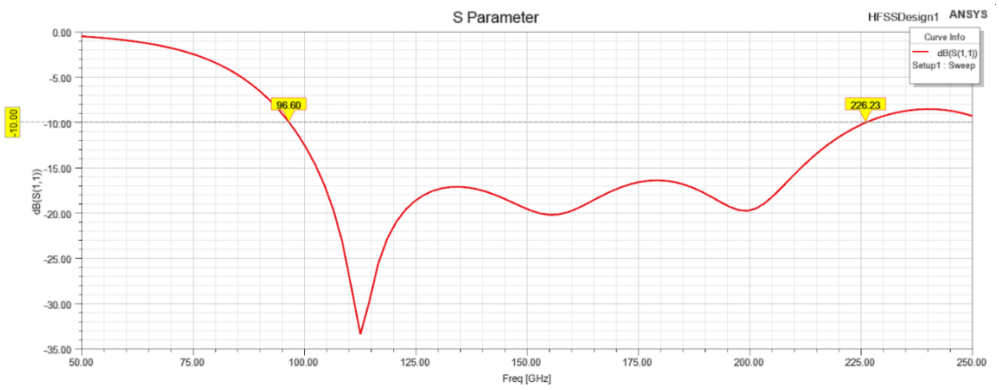

Figure 5.2 S-parameter of planar monopole antenna

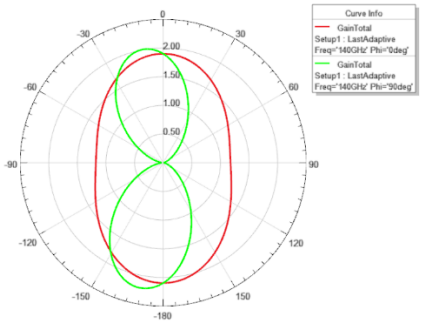

Figure 5.3 Radiation pattern of planar monopole antenna at 140 GHz

As indicated in [13], planar and printed monopole antennas are the good candidates for use in UWB wireless technology because of their wide impedance bandwidth and nearly omni-directional azimuthal radiation pattern. The phenomenon of large impedance bandwidth in planar monopole antenna can be explained by the theory of microstrip patch antennas. The planar monopole antenna can be conceptualized as a microstrip patch antenna with ground plane located at an infinite distance from the substrate. The space between the infinitely far ground plane and the quartz substrate can be treated as an infinite thick air dielectric substrate. As [12] indicated, the bandwidth of the microstrip patch antenna is inversely proportional to the thickness of the substrate. Consequently, thick air dielectric substrate contributes to the broad bandwidth of the planar monopole antenna. Although this conceptualization helps explain the broad impedance bandwidth of planar monopole antennas, it falls short when applied to actual wideband antenna design, as it does not account for gain loss due to increased substrate thickness. For thick substrates, losses from surface waves become significant and must be considered, [2]. Those surface waves will hurt the net antenna gain [14].

Parameter sweeping is necessary for antenna performance optimization. In [10], some parameters that influence the antenna performance are investigated, including the CPW signal trace width, the radius of the ground plane. In this thesis, following the design procedure in [10], some parameters, including d, W_p and L_p are swept and discussion about them are shown as follows:

1) d. d is the gap between the patch and the ground plane. Its value is small compared to the dimension of the radiating patch which will introduce coupling effect for the current distribution in the patch and the ground plane. The current distribution for ground plane and radiating patch is configured as Figure (5.4) and the maximum current concentrates around the gap, leading to the appearance of inductive current. In [10], the shapes of two ground planes in CPW are adjusted for better impedance matching. During the design procedure of the proposed antenna in [10], d is changed, such as changing rectangle shape ground plane into quarter-circular ground plane and adjust radius of the quarter-circular ground plane. The simulation results in [10] indicates that d dramatically affects the matching. The parametric sweeping for d is investigated in this thesis for verification. The simulation result is shown as Figure (5.5). As d sweeps, the resonant frequencies change correspondingly. Higher band resonant frequency increases and the lower band resonant frequency decreases, which leads to the increase of the bandwidth. In this thesis, $d = 50\mu m$ is selected to get a -15 dB margin within the frequency window starting from 120 GHz to 160 GHz.

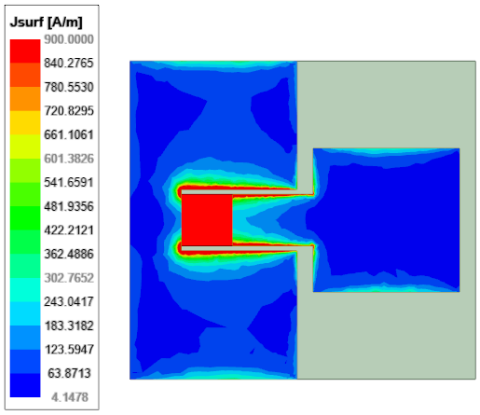

Figure 5.4 Current distribution of planar monopole antenna at 140 GHz

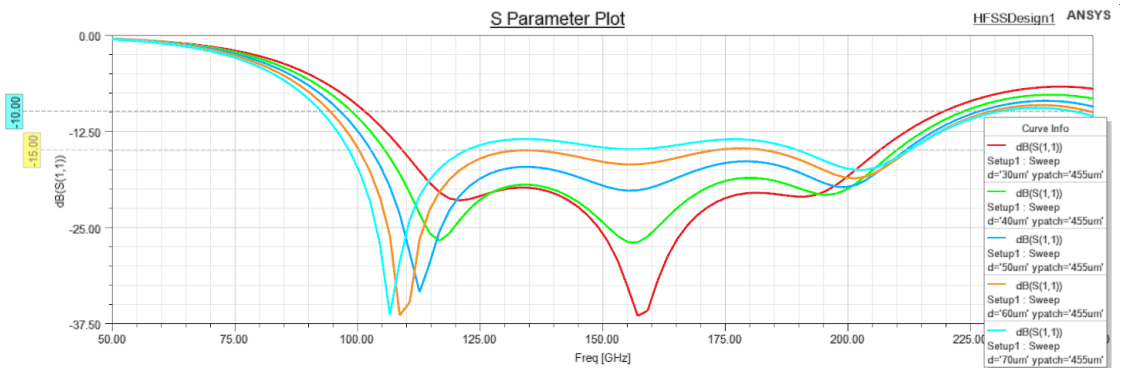

Figure 5.5 Parametric simulations of d

2) L_p. L_P is the length of the radiating patch. This parameter primarily determines the resonant frequency for quarter-wavelength monopole antenna, as stated in Equation (5.1). The S-parameter plot is illustrated as Figure 5.7. The frequency distance between two resonant frequency increases as L_P increases. Another theory is introduced in [15]. This article illustrates that the resonant frequency is inversely proportional to the summation of monopole length (L_P), gap (d) and effective radius of the equivalent cylindrical monopole (r). The relationship is illustrated as Equation (5.2).

$$f_r = \frac{c}{\lambda} = \frac{7.2}{L_p + r + d}\ GHz \tag{5.2}$$

Although there is a discrepancy between the theoretical calculations and the simulation results, the trends are consistent. The discrepancy might be caused by the operating frequency difference. Equation (5.2) is derived from measurements of low-frequency antennas (below 10 GHz). However, this thesis focuses on the millimeter-wave frequency range (above 100 GHz), where transmission modes are more complex compared to lower frequencies. However, the tendency of the resonant frequency shifting due to L_p changing is consistent for both theories and the simulation results.

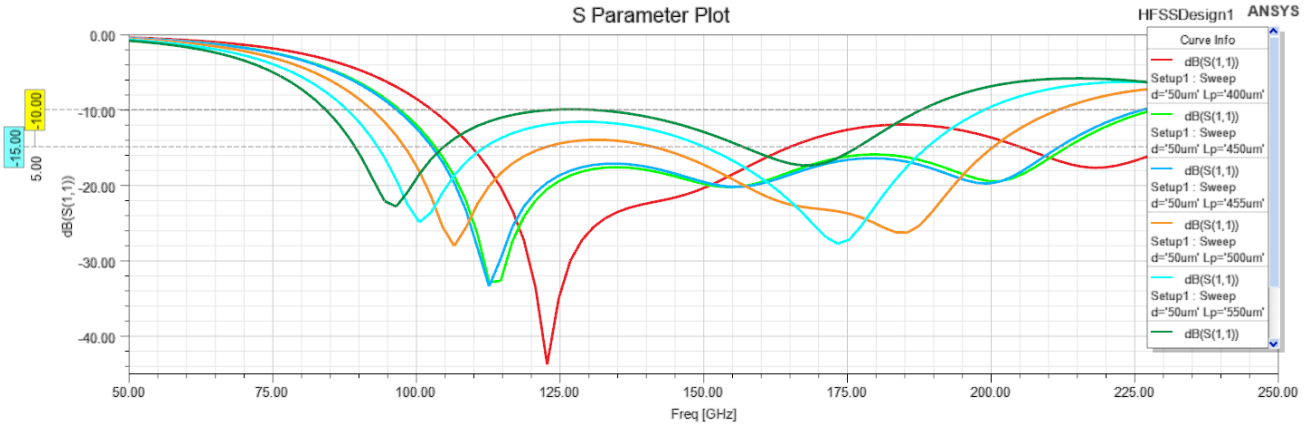

Figure 5.6 Parametric simulations of L_P

3) W_p. W_P is the width of the radiation patch. The relation between resonant frequency and the patch width W_p is illustrated as Equation (5.2) [10]. The parametric sweeping of W_p is shown as Figure (5.6). As illustrated in this figure,

the higher band resonant frequency shifts to left as W_p increases, as predicted in Equation (5.2). Also, in [15] the resonant

$$W_p = \frac{c}{2\, f_r \sqrt{\frac{\epsilon_r + 1}{2}}} \tag{5.2}$$

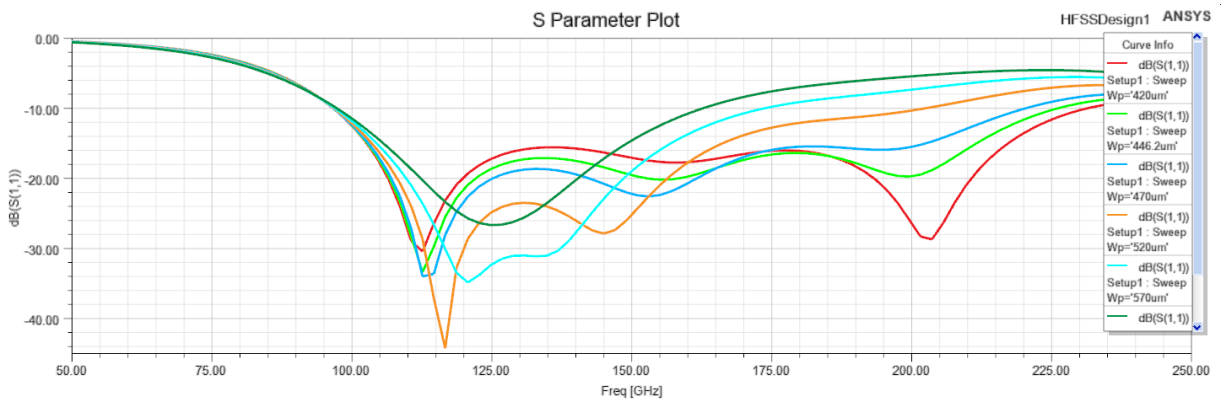

Figure 5.7 Parametric simulations of W_P

5.4 Conclusion

In this chapter, a D-band planar monopole antenna is introduced. This antenna has impressive wide bandwidth. Some parametric sweepings demonstrate the influence on impedance matching from adjustments of d, W_p, L_p. However, this antenna's gain is not large enough for PMMW imaging. One approach is adding a ground plane at the back of the substrate, which will transfer the planar monopole antenna into a microstrip patch antenna. The next chapter will discuss the design and performance of D-band coplanar patch antenna.

Chapter 6 Coplanar Patch Antenna

6.1 Motivation

From the analysis in Chapter 5, the planar monopole antenna suffers from its low gain. To improve the gain, one method is adding an extra ground plane at the back of the substrate to reduce the radiation leakage from the back of the antenna. While this approach can significantly improve gain performance, it is important to notice that the antenna then transitions from being a CPW-fed planar monopole antenna to a GCPW-fed microstrip patch antenna. According to the discussion in Chapter 2, the microstrip patch antennas have relatively limited bandwidth compared to planar monopole antennas. Therefore, further innovation antenna structures are necessary to enhance the bandwidth performance of the microstrip patch antenna.

The coplanar patch structure exhibits a relatively wide impedance bandwidth, compared to the conventional microstrip patch antenna. As indicated in [16], the coplanar patch antenna was initially perceived as a loop slot antenna. The slot antenna is complementary to the dipole antenna. As indicated by Babinet's principle, slot antenna has complementary radiation properties to the dipole antenna. Given that dipole antennas possess a relatively large bandwidth in comparison to microstrip patch antennas, slot antennas also exhibit relatively large bandwidths according to Babinet's principle. In [17], it is concluded that CPW-fed slot loop antennas have been widely use due to several advantages, including their wider bandwidth. Consequently, the coplanar patch antenna is

more suitable for PMMW imaging system compared to the conventional microstrip patch antenna.

6.2 Design and Analysis

The proposed optimized antenna structure for the coplanar patch antenna is shown in Figure 6.1. This antenna structure consists of a radiating patch surrounded by an extended ground and a coplanar waveguide with ground (GCPW) serving as the transmission line. A U-slot is incorporated into the patch to enhance impedance matching. The substrate uses a quartz with $300\mu m$ thickness and its dimension are $2260\mu m \times 1788\mu m$. Compared to the planar monopole antenna in Chapter 5, the thickness of the substrate has been increased to improve the bandwidth performance of the antenna. As previously mentioned, the microstrip patch antenna is limited by its low impedance bandwidth. Increasing the substrate thickness has been shown to positively impact impedance bandwidth performance [12]. In actual parametric sweeping, with the thickness increasing, the adjacent S-parameter points on the Smith chart become closer when the frequency is swept. Through optimization, $300\mu m$ thickness quartz was found to provide sufficiently wide impedance bandwidth, making it suitable for patch antenna design. The optimal parameters of the antenna are detailed in Table 6.1.

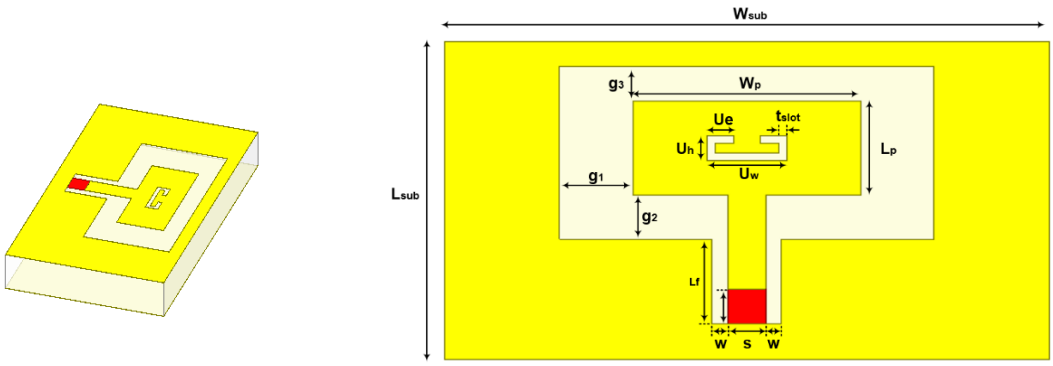

Figure 6.1 Designed coplanar patch antenna for passive imaging signal receiving.

Parameter	Value (μm)	Parameter	Value (μm)
W_{sub}	2260	L_{sub}	1130
W_p	850	L_p	375
L_f	340	g_1	275
g_2	175	g_3	138
w	60	s	140
U_w	300	U_h	100
U_e	150	t_{slot}	30

Table 6.1 Parameters for coplanar patch antenna

The coplanar patch behaves like a "patch" around the resonant point [16]. The length (L_p) of the patch is around $0.5\lambda/\sqrt{\epsilon_r}$. The E field of the patch behaves the same as the microstrip patch antenna (Figure 6.2). According to the cavity model for microstrip patch antenna, the E field along two feed side and the outer side of the patch have

opposite directions since the electromagnetic wave in microstrip patch antenna propagating in TM_{010} mode. For impedance matching, [16] demonstrated that the input impedance of the coplanar patch antenna can be adjust by changing the width (W_p) of the patch. This rule is verified by parametric sweeping as illustrated in Figure 6.3. The contour of S_{11}in the smith chart vary with W_p sweeping. When $W_p = 850\ \mu m$, the contour has the smallest radius which is the optimal value for W_p.

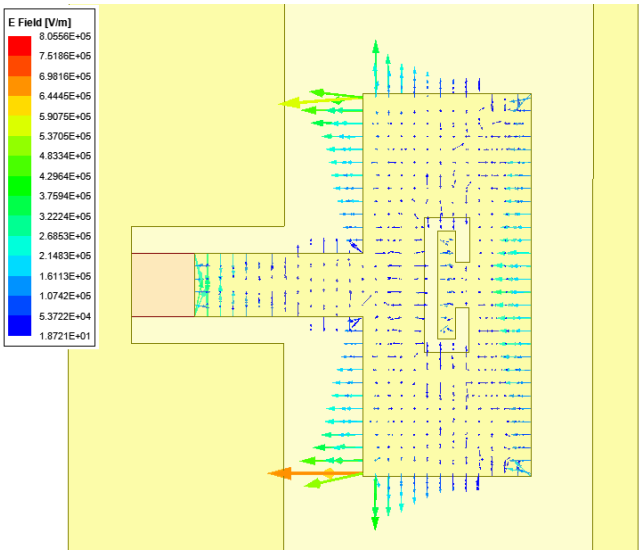

Figure 6.2 E field distribution of patch

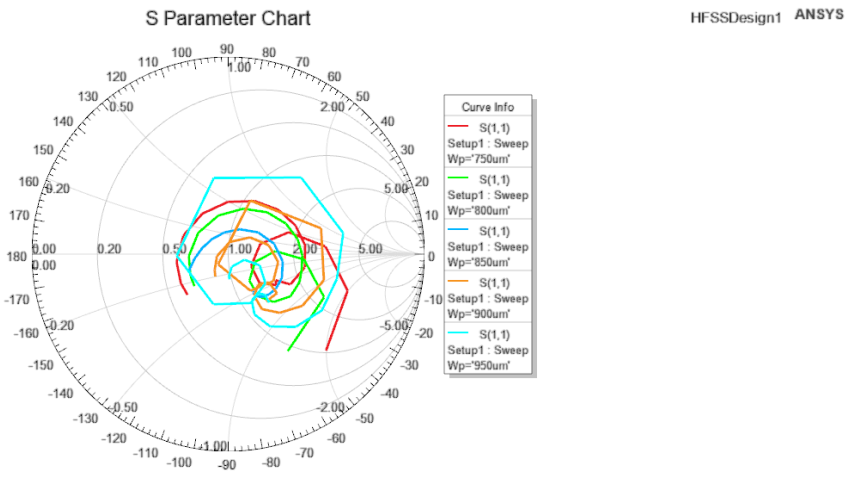

Figure 6.3 Parametric simulations of W_P in coplanar patch antenna

During the process of parametric sweeping, it is crucial to consider not only impedance matching but also the radiation pattern's directivity, given the gain requirements for passive imaging receiving. It is always preferred to have maximum gain at the position where $\theta = 0°$. As observed in Figure 6.2, the E-field distribution in the horizontal plane resembles that of a microstrip patch antenna, allowing the same theoretical principles to be applied to the proposed coplanar patch antenna. Similar to the microstrip patch antenna, two edges of the patch with the length equals to W_p primarily contribute to radiation. However, different from the microstrip patch antenna, the gap between patch and the ground plane ($g_2 and\ g_3$) predominantly determines the shape of the radiation pattern. When $g_2 and\ g_3$ are swept, the radiation pattern will be varied as well. Figure 6.4-a to 6.4-c shows two scenarios where the gaps ($g_2 and\ g_3$) have been altered. Compared to Figure 6.1, the gain in Figure 6.4-a when $\theta = 0°$ is low, the two maximum radiation lobes, indicated in red, are separated. The difference between two

antennas is the gap distance. Gap distance ($g_2 and\ g_3$) in Figure 6.4-a is much smaller than that in Figure 6.1. As an extreme case, one part of the ground plane is removed as shown in Figure 6.4-b. It is noticeable that radiation pattern at corresponding direction dramatically decreases. This can be explained by the microstrip patch cavity model, where the gaps ($g_2 and\ g_3$) in the coplanar patch antenna function similarly to the gaps between patch and back ground plane in the microstrip patch antenna. Based on this observations, parametric sweepings about $g_2 and\ g_3$ are conducted to optimize the shape of the radiation pattern. For Figure 6.4-c, the optimal structure and its radiation patterns are illustrated. The radiation patterns remain nearly identical within the 125 GHz to 162 GHz frequency window. At both 125 GHz and 162 GHz, the maximum gain occurs at $\theta = 0$ °, which is highly desirable for this project. Although the maximum gain at 140 GHz does not occur exactly at $\theta = 0$ °, it is close to the maximum value, as illustrated in Figure 6.7. This optimized antenna structure provides a relatively large and consistent gain at $\theta = 0$ ° from 125 GHz to 162 GHz, making it particularly advantageous.

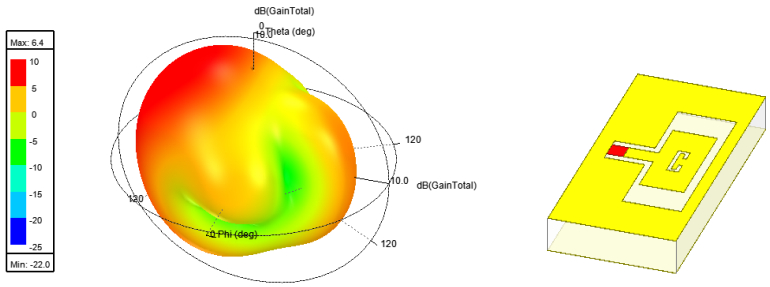

Figure 6.4-a Radiation pattern of coplanar patch antenna with $g_2\ and\ g_3$ changed.

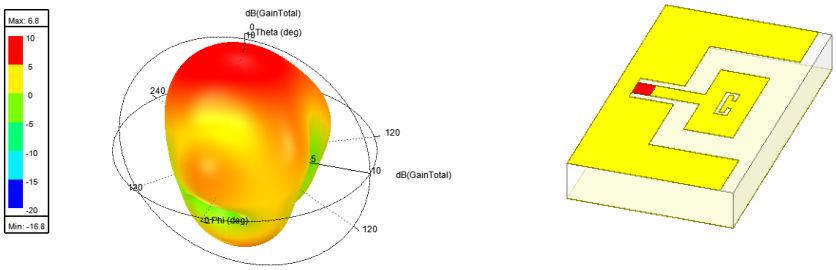

Figure 6.4-b Radiation pattern of coplanar patch antenna with top ground plane removed

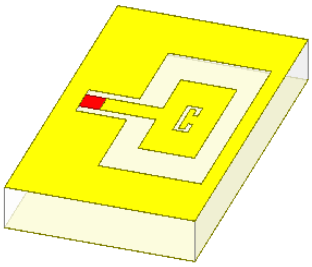

(a) Optimized antenna

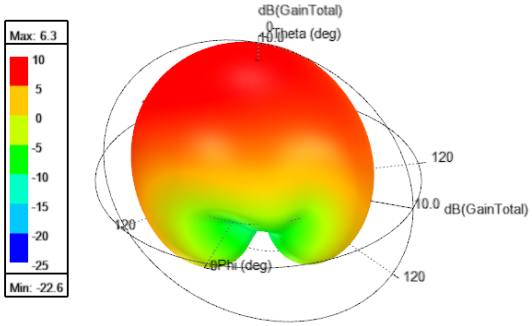

(b) Radiation pattern at 125 GHz

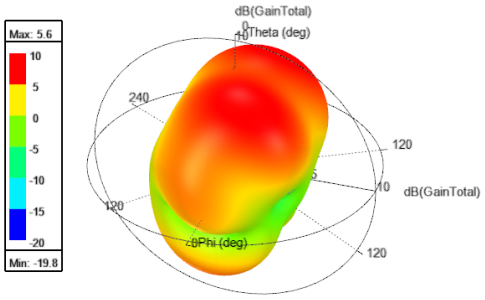

(c) Radiation pattern at 140 GHz

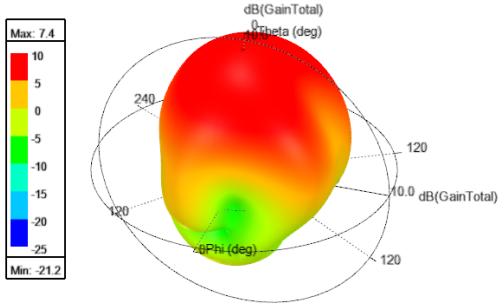

(d) Radiation pattern at 162 GHz

Figure 6.4-c Radiation pattern of coplanar patch antenna with optimal gap values

In [18], the detailed procedure for incorporating a U-slot to enhance the impedance bandwidth of a microstrip patch antenna is described. A coplanar patch antenna without the U-slot is shown Figure 6.5-a. Figure 6.5-b illustrates the S-parameter (120 GHz to 160 GHz) in Smith Chart. The contour indicates that this antenna's bandwidth does not sufficiently cover the desired D-band window. The impedance bandwidth is improved as illustrated in Figure 6.7. The slot length is set to $\frac{\lambda_g}{2} = \frac{\lambda_0}{2\sqrt{\epsilon_{eff}}}$ whereλ_g is the wavelength within the substrate and λ_0 is the free-space wavelength. In the proposed design, $2U_h + 2U_e + U_w = 800\mu m$, which is close to the half-wavelength. In [18], it is demonstrated that there is coupling between the patch resonator and the U-slot, as illustrated in Equation (6.1). Given that the designed resonant frequencies of the patch and the U-slot are identical (w_0), the coupling effect causes the two resonant frequencies to separate, resulting in two different resonant frequencies for the patch with the U-slot. These frequencies are denoted by $w_{\pm}$, representing two coupled resonant frequencies.

$$w_{\pm} = w_0\left(1 \pm \frac{U_w}{2W}\right) \tag{6.1}$$

Equation (6.3) shows that the coupling effect is influenced by the shape of the U-slot. Through parametric sweeping, all slot parameters are fine-tuned, resulting bandwidth of the proposed antenna is sufficiently wide for PMMW imaging. Figure 6.6 (a) and (b) demonstrate the case with unrefined U-slot ($U_h = 75\mu m$).

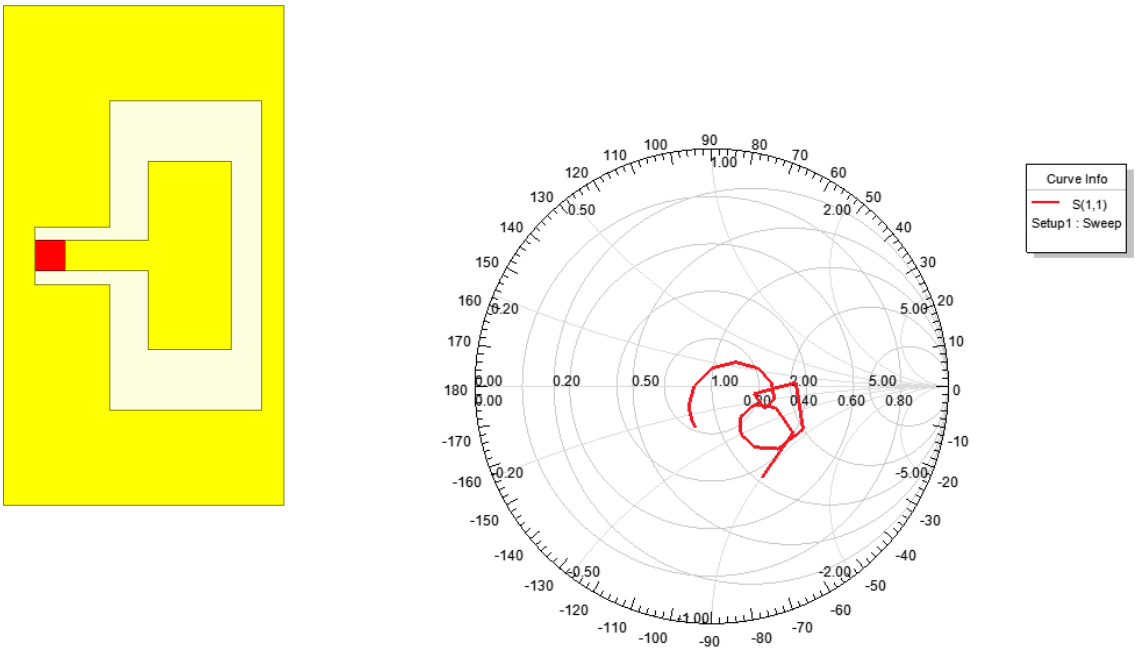

(a) Coplanar patch antenna without U-slot

(b) S-parameter of coplanar patch antenna without U-slot in 120 GHz to 160 GHz window

Figure 6.5 Coplanar patch antenna without U-slot and its S-parameter

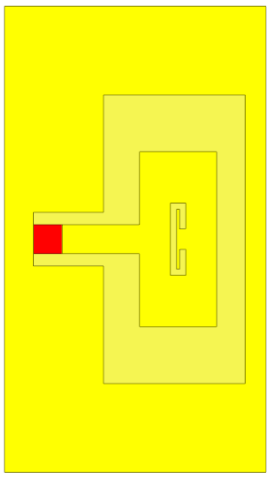

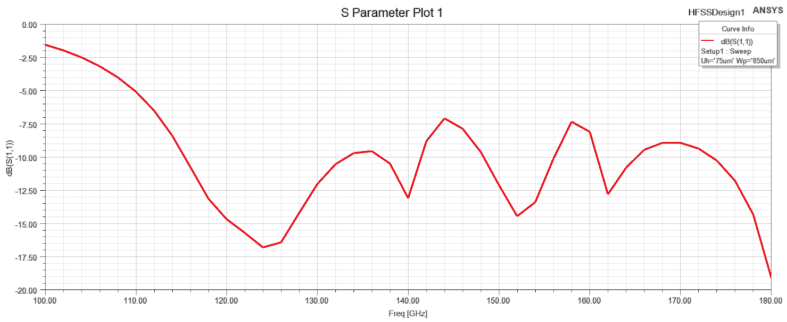

(a) Coplanar patch antenna with unrefined U-slot

(b) S-parameter of coplanar patch antenna with unrefined U-slot from 100 GHz to 180 GHz

Figure 6.6 Coplanar patch antenna with unrefined U-slot and its S-parameter

As illustrated in Figure 6.7, the proposed planar patch antenna achieves a 49.15 GHz (from 115.56 GHz to 164.71GHz) -10dB bandwidth. The corresponding gain plot is shown in Figure 6.8. For wideband antenna designs, it is essential that the gain remains sufficiently high across the desired frequency range. The proposed design provides a gain higher than 4.8 dBi. Within the 120 GHz to 160 GHz frequency, maximum gain happens at 160 GHz with value of 7.1 dBi. Compared with the planar monopole antenna, the coplanar patch antenna has better performance in gain while providing a wide enough impedance bandwidth for PMMW imaging applications. The radiation pattern of the coplanar patch antenna, as shown as the Figure 6.9, demonstrates that the radiation from the back of the antenna is effectively reduced, attributed to the presence of the ground plane.

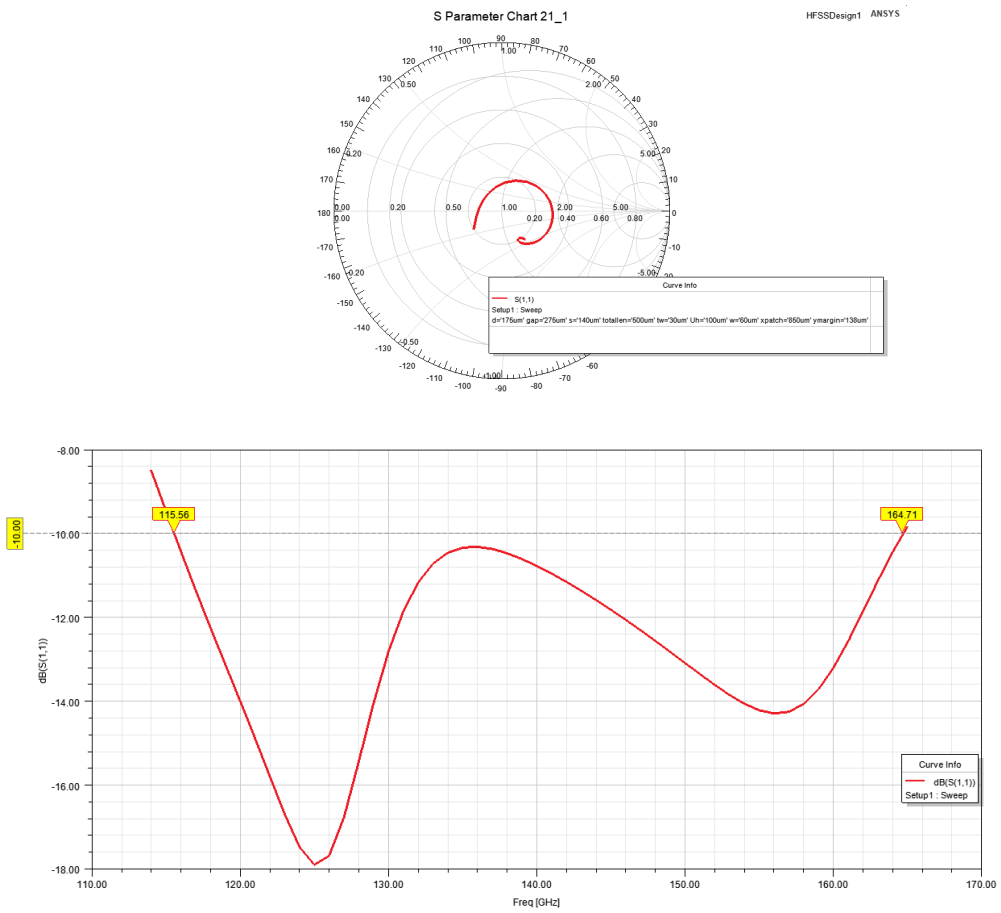

Figure 6.7 S-parameter of coplanar patch antenna

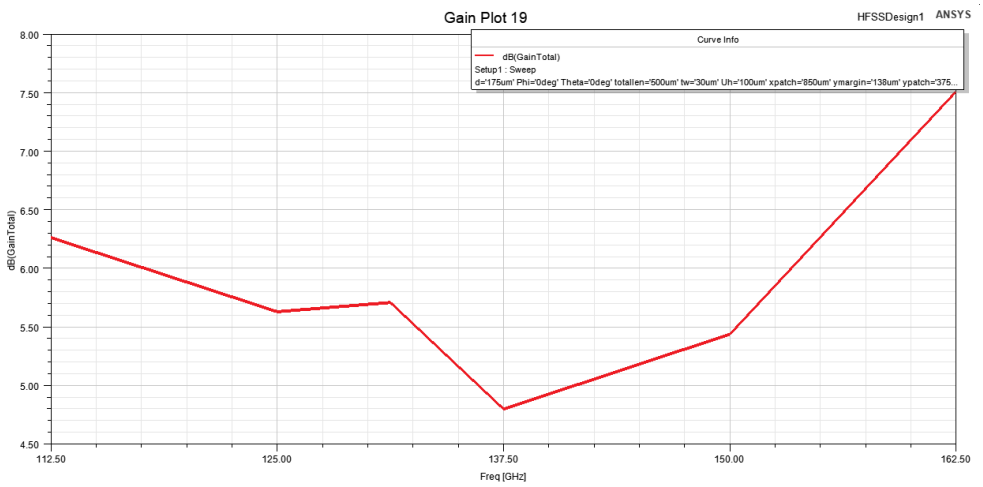

Figure 6.8 Gain plot of coplanar patch antenna

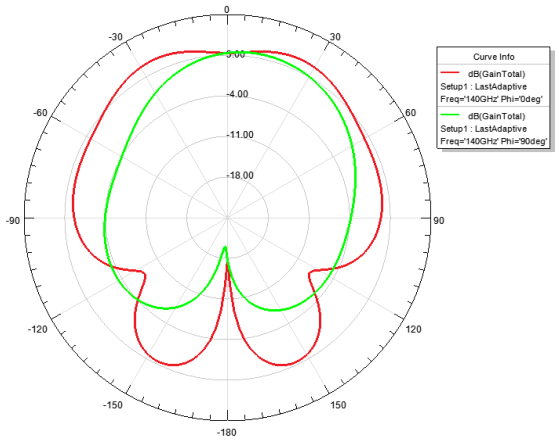

Figure 6.9 Radiation pattern of coplanar patch antenna

6.3 Conclusion

In this chapter, an improved planar antenna is proposed, which is the coplanar patch antenna. This antenna structure has good gain performance and wide bandwidth, which is suitable for PMMW imaging. Some parameters are important during the design procedure. The length of the patch (L_p) mainly determine the resonant frequency of the patch. The width of the patch (W_p) can be varied for impedance matching. Gaps between the patch and the ground plane ($g_2 and\ g_3$) will dramatically affect the radiation pattern, which need carefully adjustments before the impedance matching. Moreover, a U-slot is added on the patch to achieve wide impedance bandwidth.

Chapter 7 Conclusion and Future Work

This work presents two planar wideband antenna designs for passive imaging receiving. The planar monopole antenna offers a 129 GHz bandwidth. However, the gain of this antenna is limited due to the undesired radiation leakage from the back of the antenna. The coplanar patch antenna is proposed to mitigate that radiation leakage. The coplanar patch antenna can achieve 49.15 GHz impedance bandwidth with minimum gain higher than 4.8 dBi within that frequency range. These designs provide practical solutions for planar antennas in passive imaging applications.

One of the primary challenges in passive millimeter-wave (PMMW) imaging systems is increasing antenna gain within the desired frequency window. Future research could explore the construction of antenna arrays based on coplanar patch antenna to further enhance the antenna gain for PMMW imaging.

Characteristic Mode Analysis is used to analyze the resonant modes of the antenna. This technique transforms the antenna structures into complex matrices, which are then decomposed into orthogonal vectors known as characteristic modes. During the antenna design process, characteristic mode analysis provides variable insights into resonant frequencies and optimal feed locations to activate specific modes, thereby enabling a more systematic and efficient analysis of the antenna's operating status, which is a powerful assistance for systematic wideband antenna analysis. However, for D-band antennas, CMA requires more detailed meshing to improve the accuracy of the analysis.

Due to computational limitations, the characteristic mode analysis conducted on the proposed antennas in this study may lack precision. There is a paucity of examples of characteristic mode analysis employed in D-band or higher frequency antennas, making the analysis less systematic and efficient. Advancing the application of characteristic mode analysis to D-band wideband antenna would be significant improvement for PMMW imaging.

Reference

[1] L. Yujiri, M. Shoucri, and P. Moffa, “Passive millimeter wave imaging,” *IEEE Microwave Magazine*, vol. 4, no. 3, pp. 39–50, 2003, doi: 10.1109/MMW.2003.1237476.

[2] C. A. Balanis, *Antenna Theory: Analysis and Design*. Wiley, 2015. [Online]. Available: https://books.google.com/books?id=PTFcCwAAQBAJ

[3] D. M. Pozar, *Microwave Engineering*. Wiley, 2012. [Online]. Available: https://books.google.com/books?id=JegbAAAAQBAJ

[4] I. Bahl, M. Bozzi, and R. Garg, *Microstrip Lines and Slotlines*, Third Edition. Artech House, 2013.

[5] J. Pathak and R. Labade, “Comparative analysis of microstrip feed, CPW feed & ACS feed UWB antenna,” in *2017 International Conference on Data Management, Analytics and Innovation (ICDMAI)*, 2017, pp. 285–289. doi: 10.1109/ICDMAI.2017.8073526.

[6] A. Altaf and M. Seo, “A Review of the D-band Antennas,” in *2022 14th Global Symposium on Millimeter-Waves & Terahertz (GSMM)*, 2022, pp. 16–18. doi: 10.1109/GSMM53818.2022.9792346.

[7] C. Ma, S. Ma, L. Dai, Q. Zhang, H. Wang, and H. Yu, “Wideband and High-Gain D-Band Antennas for Next-Generation Short-Distance Wireless Communication Chips,” *IEEE Transactions on Antennas and Propagation*, vol. 69, no. 7, pp. 3700–3708, 2021, doi: 10.1109/TAP.2020.3044365.

[8] T. H. Jang, H. Y. Kim, S. H. Kim, D. M. Kang, and C. S. Park, "120 GHz On-Board Chip-to-Chip Wireless Link Using Y-Shaped Open-Ended Microstrip Antenna," *IEEE Antennas and Wireless Propagation Letters*, vol. 18, no. 10, pp. 2165–2169, 2019, doi: 10.1109/LAWP.2019.2939392.

[9] Y. Dong, T. K. Johansen, V. Zhurbenko, and P. J. Hanberg, "A Rectangular Waveguide-to-Coplanar Waveguide Transition at D-band Using Wideband Patch Antenna," in *2018 48th European Microwave Conference (EuMC)*, 2018, pp. 1045–1048. doi: 10.23919/EuMC.2018.8541505.

[10] A. El Yassini, S. Ibnyaich, S. Chabaa, and A. Zeroual, "Miniaturized broadband-multiband planar antenna with a symmetric quarter-circular ground plane for WLAN/WiMAX standards," *Microwave and Optical Technology Letters*, vol. 62, no. 9, pp. 2953–2964, 2020, doi: https://doi.org/10.1002/mop.32402.

[11] M. J. Ammann, "Square planar monopole antenna," in *IEE National Conference on Antennas and Propagation,* 1999, pp. 37–40. doi: 10.1049/cp:19990010.

[12] K. C. Gupta, "Broadbanding techniques for microstrip patch antennas-a review".

[13] Z. Hamouda, J. Wojkiewicz, A. A. Pud, L. Kone, S. Bergheul, and T. Lasri, "Flexible UWB organic antenna for wearable technologies application," *IET Microwaves, Antennas & Propagation*, vol. 12, no. 2, pp. 160–166, 2018, doi: https://doi.org/10.1049/iet-map.2017.0189.

[14] S. F. Mahmoud and Y. M. M. Antar, "Study of surface waves on planar high gain leaky wave antennas," in *2010 IEEE Antennas and Propagation Society International Symposium*, 2010, pp. 1–4. doi: 10.1109/APS.2010.5561276.

[15] K. P. Ray, “Design Aspects of Printed Monopole Antennas for Ultra-Wide Band Applications,” *International Journal of Antennas and Propagation*, vol. 2008, no. 1, p. 713858, 2008, doi: https://doi.org/10.1155/2008/713858.

[16] K. Li, C. H. Cheng, T. Matsui, and M. Izutsu, “Simulation and experimental study on coplanar patch and array antennas,” in *2000 Asia-Pacific Microwave Conference. Proceedings (Cat. No.00TH8522)*, 2000, pp. 1411-. doi: 10.1109/APMC.2000.926100.

[17] C.-P. Lai, S.-C. Chiu, P. Hsu, and S.-Y. Chen, “On the Fundamental Resonance of Slot Loop Antenna Inductively Fed by a Coplanar Waveguide,” *IEEE Transactions on Antennas and Propagation*, vol. 61, no. 12, pp. 6191–6195, 2013, doi: 10.1109/TAP.2013.2281351.

[18] J. J. Borchardt and T. C. Lapointe, “U-Slot Patch Antenna Principle and Design Methodology Using Characteristic Mode Analysis and Coupled Mode Theory,” *IEEE Access*, vol. 7, pp. 109375–109385, 2019, doi: 10.1109/ACCESS.2019.2933175.